Nature
February 2018, Volume 554 Pages 515-518
http://dx.doi.org/10.1038/nature25493
http://archimer.ifremer.fr/doc/00426/53783/

Meridional overturning circulation conveys fast acidification to the deep Atlantic Ocean

Perez Fiz F [1, *], Fontela Marcos [1], Garcia-Ibanez Maribel I. [1], Mercier Herle [2], Velo Anton [1], Lherminier Pascale [3], Zunino Patricia [2], De La Paz Mercedes [1], Alonso-Pérez Fernando [1], Guallart Elisa F. [1], Padin Xose A. [1]

[1] Instituto Investigaciones Marinas (IIM, CSIC), calle Eduardo Cabello, 6, 36208, Vigo, Spain
[2] Centre National de la Recherche Scientifique (CNRS), Ifremer, Université de Brest, Institut de Recherche pour le Développement, Laboratoire d'Océanographie Physique et Spatiale (LOPS), Centre Ifremer de Bretagne, 29280, Plouzané, France

* Corresponding author : Fiz F. Perez, email address : fiz.perez@iim.csic.es

Abstract :

Since the Industrial Revolution, the North Atlantic Ocean has been accumulating anthropogenic carbon dioxide (CO2) and experiencing ocean acidification1, that is, an increase in the concentration of hydrogen ions (a reduction in pH) and a reduction in the concentration of carbonate ions. The latter causes the 'aragonite saturation horizon'—below which waters are undersaturated with respect to a particular calcium carbonate, aragonite—to move to shallower depths (to shoal), exposing corals to corrosive waters2,3. Here we use a database analysis to show that the present rate of supply of acidified waters to the deep Atlantic could cause the aragonite saturation horizon to shoal by 1,000–1,700 metres in the subpolar North Atlantic within the next three decades. We find that, during 1991–2016, a decrease in the concentration of carbonate ions in the Irminger Sea caused the aragonite saturation horizon to shoal by about 10–15 metres per year, and the volume of aragonite-saturated waters to reduce concomitantly. Our determination of the transport of the excess of carbonate over aragonite saturation (xc[CO32−])—an indicator of the availability of aragonite to organisms—by the Atlantic meridional overturning circulation shows that the present-day transport of carbonate ions towards the deep ocean is about 44 per cent lower than it was in preindustrial times. We infer that a doubling of atmospheric anthropogenic CO2 levels—which could occur within three decades according to a 'business-as-usual scenario' for climate change4—could reduce the transport of xc[CO32−] by 64–79 per cent of that in preindustrial times, which could severely endanger cold-water coral habitats. The Atlantic meridional overturning circulation would also export this acidified deep water southwards, spreading corrosive waters to the world ocean.

Atmospheric CO_2 has increased from 280 to 400 parts per million (ppm) since the Industrial Revolution. The global ocean has captured ~30% of this anthropogenic CO_2 (C_{ant}), acting as a climate regulator[1]. This CO_2 absorption has led to a decrease in seawater

pH (~0.12 units) and in the supersaturation of $CaCO_3$ (effects collectively known as ocean acidification – OA). OA can particularly affect marine calcifiers[1] by favouring the solubility of $CaCO_3$-based shells and skeletons[2]. Notably, deep cold-water coral (CWC) reefs formed by scleractinian corals, such as the ecosystem engineer specie *Lophelia pertusa*, are highly vulnerable to OA[3]. The global distribution of CWC seems to be partly limited by the depth of the ASH, which is the boundary between aragonite-stable waters above and dissolution-prone waters below[5]. In pre-industrial times, more than 95% of CWC locations were found above the ASH[6], providing evidence that environments located below the ASH are hostile to CWC growth. In the North Pacific (NP; Fig. 1a), where the ASH is only 500 m deep[7], the distribution of aragonitic CWC is patchy and CWC do not develop to large deep reef frameworks that are abundant in the North Atlantic (NA)[8] where the ASH is deeper than 2000 m. OA is causing the ASH to shoal, thus exposing CWC to $CaCO_3$ undersaturation. Although laboratory experiments suggest that adult *L. pertusa* can acclimatize to $CaCO_3$ undersaturation[9,10], the long-term survival of CWC reefs in undersaturated water is questioned because *L. pertusa* skeleton becomes weaker when exposed yearlong to future OA scenarios[10], and the dead skeletal framework that supports the reef itself is likely to dissolve in undersaturated waters[11].

To determine the degree of aragonite saturation of the world ocean waters, we calculated $_{xc}[CO_3^{2-}]$ (in µmol kg^{-1}) by using quality-controlled global datasets of marine CO_2 system measurements[12,13]. Positive (negative) $_{xc}[CO_3^{2-}]$ indicates aragonite supersaturated (undersaturated) waters (see Methods). High positive $_{xc}[CO_3^{2-}]$ values occur in the NA while negative values occur in the NP, which is consistent with the distribution of CWC[14] below 1,000 m (Fig. 1a). About 61% (78%) of CWC found deeper than 1,000 m (1,500 m) are located in the NA where $_{xc}[CO_3^{2-}] > 0$, with an average $_{xc}[CO_3^{2-}]$ of 24.5 µmol kg^{-1} (15 µmol kg^{-1}) that is half the natural (pre-industrial) $_{xc}[CO_3^{2-}]$ (see Extended Data Table 1). The AMOC created the favourable conditions for CWC growth found in the NA by conveying ventilated waters loaded with relatively high pH and positive $_{xc}[CO_3^{2-}]$ to the deep Atlantic Ocean.

In the centre of the Irminger Sea (Fig. 1b), winter deep-convection and associated deep injection of OA recorded during 1991–2016 showed a constant increase in C_{ant} from 30 to 50 µmol kg^{-1} in the ventilated Subpolar Mode Water (Fig. 2a). During the same period, the atmospheric C_{ant} grew from 85 to 123 ppm. A thick layer of low salinity (< 34.91) traces the strong convection events that occurred during the first half of the 1990s and during 2014–2016. During those strong convection events, Subpolar Mode Water was ventilated down to 1,500 m, showing high temporal variability and no indication of a slowing-down of deep convection[15,16]. Present-day surface ocean shows an increase of about 30% in $[H^+]$ with respect to the natural (pre-industrial) value[1]. At the centre of the Irminger Sea, the $[H^+]$ increase affects a layer ~1,500 m thick (Fig. 2c), the deepest signal of direct injection of OA ever observed. Since 2002, the anthropogenic perturbation caused a deepening of the isolines of 25 and 30% of anthropogenic $[H^+]$ from surface to 1,500 m. The isolines of $_{xc}[CO_3^{2-}]$ progressively ascend at about 10–15 m yr^{-1} (Fig. 2b), with some slightly faster ascension periods related to deep convection events (arrows in Fig. 2b). The effect of these deep convection events is buffered by the partial balance between the increase in the anthropogenic $[H^+]$ and the decrease in the natural $[H^+]$ (due to the removal of the natural CO_2 accumulated in old waters by remineralisation of organic matter) (Fig. 2c). Because of this biogeochemical feedback, the decrease in $_{xc}[CO_3^{2-}]$ and the associated shoaling of the ASH are only weakly sensitive to the intensity of the deep convection.

West of 20ºW in the subpolar NA (SPNA), the ASH observed in 2016 is 200–500 m shallower than the pre-industrial ASH (Fig. 1c). Along the 2016 Ovide section, the 25 µmol kg^{-1} isoline of the present-day $_{xc}[CO_3^{2-}]$ runs close to the 50 µmol kg^{-1} isoline of natural $_{xc}[CO_3^{2-}]$, indicating a 50% decrease in the availability of CO_3^{2-} for deep CWC. These changes reflect the spreading of newly ventilated Subpolar Mode Water with low $_{xc}[CO_3^{2-}]$ from the Irminger Sea to the Iceland basin.

The 2002–2016 AMOC mean transport across the Ovide section[17] was 16.2 ± 0.8 Sv (1 Sv = 1 million m^3 s^{-1}). The upper and lower limbs of the AMOC showed contrasted $_{xc}[CO_3^{2-}]$ (Fig. 1c) and C_{ant} (Extended Data Fig. 1), with average $_{xc}[CO_3^{2-}]$ values of 61 ± 2 µmol kg^{-1} and 28 ± 3 µmol kg^{-1}, respectively. The upper limb of the AMOC flows northwards (above

the isopycnal ~1,032.15 kg m^{-3}), transporting 1,064 kmol s^{-1} of $_{xc}[CO_3^{2-}]$ (Fig. 3). About 40% of this transport (435 kmol s^{-1}) subducted into the lower limb of the AMOC in the SPNA, while the remaining 60% was exported to the Nordic Seas[18,19]. These $_{xc}[CO_3^{2-}]$ transport values are between 33 and 44% lower than the transport of natural $_{xc}[CO_3^{2-}]$ because natural $_{xc}[CO_3^{2-}]$ values in the upper and lower limbs of the AMOC (90 ± 2 and 49 ± 4 μmol kg^{-1}, respectively) are much larger than the present-day values (61 ± 2 and 28 ± 3 μmol kg^{-1}, respectively). By vertically transporting lower $_{xc}[CO_3^{2-}]$ with respect to pre-industrial, the AMOC is responsible for the decrease in pH and $_{xc}[CO_3^{2-}]$ in the deep NA.

IPCC projections[20] indicate that a warming of about 2°C will be reached when atmospheric CO_2 rises to 480–520 ppm (Extended Data Fig. 2) (i.e. a CO_2 excess over pre-industrial values or C_{ant} of 200–240 ppm). These figures are about two-fold the present-day anthropogenic perturbation in temperature and CO_2 (1ºC warming[21] and C_{ant} of 100–120 ppm). The $_{xc}[CO_3^{2-}]$ for a doubling of the atmospheric C_{ant} was inferred by adding 0.72 times present-day marine C_{ant} (Extended Data Fig. 1) to the marine $[CO_2]$ observed in 2002–2016 and assuming that C_{ant} changes follow the transient steady approximation[22,23] (see Methods). The projected slow-down of the deep convection by the end of the century should not invalidate this approach because, as concluded above, the decrease in $_{xc}[CO_3^{2-}]$ is only weakly sensitive to the intensity of the deep convection. When doubling the atmospheric C_{ant}, the volume of aragonite-saturated deep waters in the Iceland basin and the Irminger Sea decreases dramatically as shown by the 1,000–1,700 m shoaling with respect to pre-industrial depths of both the ASH and the isolines of 25–50 μmol kg^{-1} of $_{xc}[CO_3^{2-}]$ (Fig. 1c). A most striking feature is the vanishing of the vertical gradient of $[H^+]$ caused by OA (Extended Data Fig. 3), due to the relatively rapid deep injection of C_{ant} by the AMOC, leading to the homogenization of the pH in the whole water column. The disappearance of the vertical gradient of pH would lead to a substantial weakening of the vertical gradient of $_{xc}[CO_3^{2-}]$.

We find that doubling the atmospheric C_{ant} could result in 70% of the CWC deeper than 1,500 m in the NA living below the ASH and being exposed to negative $_{xc}[CO_3^{2-}]$ (Extended Data Table 1). An average reduction of 75% in $_{xc}[CO_3^{2-}]$ with respect to pre-

industrial would be observed for the CWC living below 1,000 m. This may occur as soon as 2050 in a business as usual scenario (SSP5, see Extended Data Fig. 2)[4]. Our data-based results are in line with the IPCC projections[24] that point to OA being a serious threat for deep (> 1,000 m) CWC habitats in the NA by 2100. However, most recent model studies showed large discrepancies in their estimates of the extent of CWC habitats that could be exposed to corrosive waters by the end of the century. The proportion of CWC projected to live below the ASH varies between 23% and 70% of its present-day area for the most recent simulations using business as usual concentration pathways[6,25]. The portion could reach 85% of the Northeast Atlantic CWC surfaces by 2060[26]. Our findings support the latter projection. We show that the water masses of the lower limb of the AMOC are becoming more acidic. Those water masses are ventilating the deep layers of the world ocean and propagating the acidification threat to the CWC habitats of the world ocean. We estimate that for a doubling of the atmospheric C_{ant}, the average $_{xc}[CO_3^{2-}]$ below 1,000 m would become negative for the world ocean (Extended Data Table 1), indicating that most of the deep CWC habitats of the world ocean may be exposed to corrosive waters by 2050.

Models predict a slow-down of 25% of the mid-latitude AMOC by the end of the present century[20], which would lead directly to decreasing volume of the southward export of waters with negative $_{xc}[CO_3^{2-}]$ to the global deep ocean. However, the AMOC reduction would also lead to a reduction of the ventilation of the deep ocean at mid-latitudes and, therefore, to a reduction of the dissolved oxygen and pH through remineralisation processes[27–29]. Therefore, future AMOC slow-down could contribute to worsen the acidification threats for deep CWC.

REFERENCES:

1. Gattuso, J.-P. *et al.* Contrasting futures for ocean and society from different anthropogenic CO_2 emissions scenarios. *Science* **349,** aac4722 (2015).
2. Pörtner, H.-O. *et al.* Ocean systems. in *Climate Change 2014: Impacts, Adaptation, and Vulnerability. Part A: Global and Sectoral Aspects. Contribution of Working Group II to the Fifth Assessment Report of the Intergovernmental Panel of Climate Change* (eds. Field, C. B. et al.) 411–484 (Cambridge University Press, 2014).

3. Roberts, J. M. *Cold-Water Corals: The Biology and Geology of Deep-Sea Coral Habitats*. (Cambridge University Press, 2009).
4. Riahi, K. *et al.* The Shared Socioeconomic Pathways and their energy, land use, and greenhouse gas emissions implications: An overview. *Glob. Environ. Change* **42,** 153–168 (2017).
5. Tittensor, D. P., Baco, A. R., Hall-Spencer, J. M., Orr, J. C. & Rogers, A. D. Seamounts as refugia from ocean acidification for cold-water stony corals. *Mar. Ecol.* **31,** 212–225 (2010).
6. Guinotte, J. M. *et al.* Will human-induced changes in seawater chemistry alter the distribution of deep-sea scleractinian corals? *Front. Ecol. Environ.* **4,** 141–146 (2006).
7. Jiang, L.-Q. *et al.* Climatological distribution of aragonite saturation state in the global oceans. *Glob. Biogeochem. Cycles* **29,** 1656–1673 (2015).
8. Feely, R. A. *et al.* Impact of Anthropogenic CO_2 on the $CaCO_3$ System in the Oceans. *Science* **305,** 362–366 (2004).
9. Maier, C., Hegeman, J., Weinbauer, M. G. & Gattuso, J.-P. Calcification of the cold-water coral Lophelia pertusa, under ambient and reduced pH. *Biogeosciences* **6,** 1671–1680 (2009).
10. Hennige, S. J. *et al.* Hidden impacts of ocean acidification to live and dead coral framework. *Proc. R. Soc. B Biol. Sci.* **282,** 20150990 (2015).
11. Thresher, R., Tilbrook, B., Fallon, S., Wilson, N. & Adkins, J. Effects of chronic low carbonate saturation levels on the distribution, growth and skeletal chemistry of deep-sea corals and other seamount megabenthos. *Mar. Ecol. Prog. Ser.* **442,** 87–99 (2011).
12. Olsen, A. *et al.* The Global Ocean Data Analysis Project version 2 (GLODAPv2) – an internally consistent data product for the world ocean. *Earth Syst. Sci. Data* **8,** 297–323 (2016).
13. Key, R.M. *et al. Global Ocean Data Analysis Project, Version 2 (GLODAPv2), ORNL/CDIAC-162, ND-P093*. (Carbon Dioxide Information Analysis Center (CDIAC), 2015).
14. Freiwald, A., Fosså, H., Grehan, A., Koslow, T. & Roberts, J. M. *Cold-water coral reefs: out of sight-no longer out of mind*. **22,** (UNEP-WCMC, Cambridge, UK, 2004).

15. Pickart, R. S. *et al.* Convection in the Western North Atlantic Sub-Polar Gyre: Do Small-Scale Wind Events Matter? in *Arctic–Subarctic Ocean Fluxes* 629–652 (Springer, Dordrecht, 2008).
16. Yashayaev, I. & Loder, J. W. Further intensification of deep convection in the Labrador Sea in 2016. *Geophys. Res. Lett.* **44,** 1429–1438 (2017).
17. Mercier, H. *et al.* Variability of the meridional overturning circulation at the Greenland–Portugal OVIDE section from 1993 to 2010. *Prog. Oceanogr.* **132,** 250–261 (2015).
18. Jeansson, E. *et al.* The Nordic Seas carbon budget: Sources, sinks, and uncertainties. *Glob. Biogeochem. Cycles* **25,** GB4010 (2011).
19. Pérez, F. F. *et al.* Atlantic Ocean CO_2 uptake reduced by weakening of the meridional overturning circulation. *Nat. Geosci.* **6,** 146–152 (2013).
20. *Climate Change 2013 - The Physical Science Basis: Working Group I Contribution to the Fifth Assessment Report of the Intergovernmental Panel on Climate Change*. (Cambridge University Press, 2014).
21. Le Quéré, C. The implications of COP21 for our future climate. *Public Health Rev.* **37,** 29 (2016).
22. Tanhua, T. *et al.* Changes of anthropogenic CO_2 and CFCs in the North Atlantic between 1981 and 2004. *Glob. Biogeochem. Cycles* **20,** GB4017 (2006).
23. Steinfeldt, R., Rhein, M., Bullister, J. L. & Tanhua, T. Inventory changes in anthropogenic carbon from 1997–2003 in the Atlantic Ocean between 20°S and 65°N. *Glob. Biogeochem. Cycles* **23,** GB3010 (2009).
24. Hoegh-Guldberg, O. *et al.* The Ocean. in *Climate Change 2014: Impacts, Adaptation, and Vulnerability. Part B: Regional Aspects. Contribution of Working Group II to the Fifth Assessment Report of the Intergovernmental Panel of Climate Change* (eds. Barros, V. R. et al.) 1655–1731 (Cambridge University Press, 2014).
25. Gehlen, M. *et al.* Projected pH reductions by 2100 might put deep North Atlantic biodiversity at risk. *Biogeosciences* **11,** 6955–6967 (2014).
26. Jackson, E. L., Davies, A. J., Howell, K. L., Kershaw, P. J. & Hall-Spencer, J. M. Future-proofing marine protected area networks for cold water coral reefs. *ICES J. Mar. Sci. J. Cons.* **71,** 2621–2629 (2014).

27. Tagklis, F., Bracco, A. & Ito, T. Physically driven Patchy O2 Changes in the North Atlantic Ocean simulated by the CMIP5 Earth System Models. *Glob. Biogeochem. Cycles* doi:10.1002/2016GB005617
28. Resplandy, L., Bopp, L., Orr, J. C. & Dunne, J. P. Role of mode and intermediate waters in future ocean acidification: Analysis of CMIP5 models. *Geophys. Res. Lett.* **40,** 3091–3095 (2013).
29. Fontela, M., García-Ibáñez, M. I., Hansell, D. A., Mercier, H. & Pérez, F. F. Dissolved Organic Carbon in the North Atlantic Meridional Overturning Circulation. *Sci. Rep.* **6,** 26931 (2016).

Methods:

Aragonite saturation and carbonate ion excess

Aragonite is one of the $CaCO_3$ metastable forms used by calcifying marine organisms to build their shells[30,31]. A measure of the bioavailability of aragonite is the *in situ* degree of aragonite saturation (Ω_A) given by Eq. (1):

$$\Omega_A = \frac{[Ca^{2+}][CO_3^{2-}]_{is}}{K_A} \qquad (1)$$

where $[Ca^{2+}]$ is the concentration of the major ion calcium, $[CO_3^{2-}]$ is the concentration of the carbonate ion, and K_A is the $CaCO_3$ aragonite solubility product. Subscript "is" denotes at *in situ* temperature and pressure conditions. $[Ca^{2+}]$ is conservative and is obtained from salinity (S) through Eq. (2)[32]:

$$[Ca^{2+}] = 0.01028 \times S/35 \qquad (2)$$

Another convenient measure of the aragonite saturation is the difference between $[CO_3^{2-}]_{is}$ and the $[CO_3^{2-}]$ at saturation ($[CO_3^{2-}]_{sat(\Omega A = 1)}$), which is the excess of carbonate ion concentration over aragonite saturation ($_{xc}[CO_3^{2-}]$):

$$_{xc}[CO_3^{2-}] = [CO_3^{2-}]_{is} - [CO_3^{2-}]_{sat(\Omega A=1)} \quad (3).$$

Positive (negative) $_{xc}[CO_3^{2-}]$ indicates that water is supersaturated (undersaturated) with respect to aragonite. The $_{xc}[CO_3^{2-}]$ is an absolute measure of the tendency for the aragonite mineral to precipitate/dissolve[33] so that, contrary to the widely used Ω_A that is a ratio, it is founded to compute $_{xc}[CO_3^{2-}]$ transport. In addition, changes in $_{xc}[CO_3^{2-}]$ are directly

comparable with changes in $[CO_3^{2-}]_{is}$, which in this study was computed from total alkalinity (A_T) and total dissolved inorganic carbon (C_T). The acid dissociation constants of Dickson and Millero[34] and aragonite solubilities of Mucci[35] were selected to determine $_{xc}[CO_3^{2-}]$ and other derived variables of the marine CO_2 system using the CO2SYS toolbox[36,37].

Present, natural and projected values of $_{xc}[CO_3^{2-}]$ and $[H^+]$

Present $_{xc}[CO_3^{2-}]$ and $[H^+]$ were determined using measured data of the marine CO_2 system (A_T, C_T and pH), temperature, salinity and pressure. We separated anthropogenic from natural $_{xc}[CO_3^{2-}]$ and $[H^+]$ by assuming that the natural component corresponds to an ocean in equilibrium with a pre-industrial atmosphere, whereas the remaining is anthropogenic. Along the Ovide section, we determined the anthropogenic CO_2 (C_{ant}) using the back-calculation φC_T^o method[19,38,39] with an overall uncertainty of ±5.2 µmol kg^{-1}. For the Nordic Sills, the parameters of the marine CO_2 system were taken from Jeansson et al.[18]. Natural C_T was determined by subtracting the C_{ant} to the measured C_T. Natural $_{xc}[CO_3^{2-}]$ and $[H^+]$ were determined using measured A_T and natural C_T and the equations of the marine CO_2 system using CO2SYS toolbox[36,37].

The Shared Socio-Economic Pathways, SSP[4] (Extended Data Fig. 2), indicate that the doubling of the present atmospheric C_{ant} of 100–120 ppm, i.e. atmospheric CO_2 of 480–520 ppm (200–240 ppm over pre-industrial values), would lead to a 2ºC-warming scenario. The $_{xc}[CO_3^{2-}]$ and $[H^+]$ for this scenario were calculated by doubling the present atmospheric C_{ant}. The comparison of the observed changes in C_T and chlorofluorocarbons with those predicted from an eddy-permitting ocean circulation model confirmed that C_{ant} changes follow the transient steady state (TSS) approximation[22,23,40]. This means that C_{ant} increases over time through the whole water column proportionally to the increase in C_{ant} in the surface mixed layer. Hence, we estimated the seawater C_{ant} for the doubling of atmospheric C_{ant} from the present-day seawater C_{ant} considering that the change in the seawater surface C_{ant} follows the change in atmospheric CO_2. The seawater C_{ant} for this scenario was estimated to be 72 ± 3% higher than the present seawater C_{ant} (Extended Data Fig. 4), based on a large range of temperatures (0–20ºC) and a CO_2 air-sea disequilibrium[41] of 10 ± 5%. The $_{xc}[CO_3^{2-}]$ and $[H^+]$ for the doubling of atmospheric C_{ant} scenario were determined by

adding the 0.72 times the present seawater C_{ant} to the measured C_T and using measured A_T and temperature. $[H^+]$ is given in pmol kg^{-1} as the $\log^{-1}$ of pH_T (in total scale). The uncertainty range for the ASH for the doubling of atmospheric C_{ant} scenario (milky area in Fig. 1c) was determined considering an atmospheric CO_2 concentration of 480–520 ppm.

Present, natural and projected carbonate ion excess at cold-water coral (CWC) locations

The stony coral database was derived from records compiled by Rogers et al.[42], Hall-Spencer et al.[43] and a database of *L. pertusa* records compiled by the United Nations Environment Programme – World Conservation Monitoring Centre (UNEP-WCMC) based in the CWC Global distribution[44]. From the obtained 6,553 CWC records, we removed those without geo-referenced coordinates or depth data, those shallower than 1,000 m, and those characterized as dead or fossil, obtaining 548 CWC records (Fig. 1a and Extended Data Table 1). To determine the physicochemical characteristics of the seawater surrounding those 548 CWC locations, we used a multiparametric interpolation method (Water Mass Properties [WMP] interpolation method)[45] to interpolate *in situ* temperature, salinity, A_T and C_T from the quality controlled GLODAPv2 database[12,13]. The WMP method improves the estimates obtained from purely spatial interpolation by applying a weighting process using the distances in conservative parameters and using a helper database with higher resolution (World Ocean Atlas[46–49]) for these conservative parameters. The C_{ant} at those 548 CWC locations for 2010 was interpolated from the C_{ant} given by Khatiwala et al.[50]. Following the same procedure as that described above, the present, natural and projected ${}_{xc}[CO_3^{2-}]$ for a doubling of atmospheric C_{ant} were determined. The results are summarized in Extended Data Table 1.

Circulation of carbonate ions and anthropogenic CO_2 in the Subpolar North Atlantic

The absolute geostrophic velocity fields orthogonal to the Ovide sections were determined using an inverse model constrained by subsurface acoustic Doppler current profiler measurements and an overall mass conservation constraint[17,51–53]. The resulting absolute velocity fields are consistent with independent altimetry measurements[52] and estimates of the western boundary current transport[53] at the time of the Ovide cruises. The velocity fields are representative of the month of the cruise and the seasonal variability was removed

as explained in Pérez et al.[19]. The mean velocity field of the Ovide section during 2002–2016 is shown in Extended Data Fig. 5. Transports of $_{xc}[CO_3^{2-}]$, $[H^+]$, C_{ant} and $[CO_3^{2-}]$ were calculated using the velocity field, density and the tracer concentration ($_{xc}[CO_3^{2-}]$, $[H^+]$, C_{ant} or $[CO_3^{2-}]$) through Eq. (4):

$$\text{Transport}_{Tracer} = \Sigma\,[\text{Tracer}] * \text{density}_{\text{is}} * \text{velocity} * \text{area} \qquad (4)$$

The transports of seawater, $_{xc}[CO_3^{2-}]$, $[H^+]$, C_{ant} and $[CO_3^{2-}]$ are summarize in Extended Data Table 2, Fig. 3 and Extended Data Fig. 6. The transports of $_{xc}[CO_3^{2-}]$ and $[H^+]$ are also given for present, pre-industrial (natural) and doubling of atmospheric C_{ant} scenario. Uncertainties in the AMOC, and in the transport of $_{xc}[CO_3^{2-}]$ and $[H^+]$ trough the Ovide section were calculated as the standard error of the mean of the eight occupations of the Ovide section during 2002–2016 (s.e. = std/$\sqrt{8}$). Transport at the sills was derived from Jeansson et al.[18] and Pérez et al.[19] and results are summarized in Extended Data Table 3.

ADDITIONAL REFERENCES:

30. Fabry, V. J., Seibel, B. A., Feely, R. A. & Orr, J. C. Impacts of ocean acidification on marine fauna and ecosystem processes. *ICES J Mar Sci* **65,** 414–432 (2008).
31. Fabry, V. O. ., McClintock, J. B., Mathis, J. T. & Grebmeier, J. M. Ocean acidification at high latitudes: the bellwether. *Oceanography* **22,** 160–171 (2009).
32. Millero, F. J., Feistel, R., Wright, D. G. & McDougall, T. J. The composition of Standard Seawater and the definition of the Reference-Composition Salinity Scale. *Deep Sea Res. Part Oceanogr. Res. Pap.* **55,** 50–72 (2008).
33. Subhas, A. V. *et al.* A novel determination of calcite dissolution kinetics in seawater. *Geochim. Cosmochim. Acta* **170,** 51–68 (2015).
34. Dickson, A. & Millero, F. A comparison of the equilibrium constants for the dissociation of carbonic acid in seawater media. *Deep-Sea Res.* **34,** 1733–1743 (1987).
35. Mucci, A. The solubility of calcite and aragonite in seawater at various salinities, temperatures, and one atmosphere total pressure. *Am. J. Sci.* **283,** 780–799 (1983).
36. Lewis, E., Wallace, D. & Allison, L. *Program developed for CO2 system calculations.* (ORNL/CDIAC-105, Carbon Dioxide Information Analysis Center, Oak Ridge National Laboratory, U.S. Department of Energy, Oak Ridge, Tennessee, 1998).
37. van Heuven, S., Pierrot, D., Lewis, E. & Wallace, D. *MATLAB Program developed for CO2 system calculations.* (ORNL/CDIAC-105b, Carbon Dioxide Information Analysis Center, Oak Ridge National Laboratory, U.S. Department of Energy, Oak Ridge, Tennessee, 2009).
38. Pérez, F. F. *et al.* Temporal variability of the anthropogenic CO2 storage in the Irminger Sea. *Biogeosciences* **5,** 1669–1679 (2008).
39. Vázquez-Rodríguez, M. *et al.* Anthropogenic carbon distributions in the Atlantic Ocean: data-based estimates from the Arctic to the Antarctic. *Biogeosciences* **6,** 439–451 (2009).
40. Tanhua, T., Körtzinger, A., Friis, K., Waugh, D. W. & Wallace, D. W. R. An estimate of anthropogenic CO2 inventory from decadal changes in oceanic carbon content. *Proc. Natl. Acad. Sci.* **104,** 3037 (2007).

41. Matsumoto, K. & Gruber, N. How accurate is the estimation of anthropogenic carbon in the ocean? An evaluation of the ΔC* method. *Glob. Biogeochem. Cycles* **19,** GB3014 (2005).
42. Rogers, A. D., Baco, A., Griffiths, H., Hart, T. & Hall-Spencer, J. M. Corals on Seamounts. in *Seamounts: Ecology, Fisheries & Conservation* (eds. Pitcher, T. J. et al.) 141–169 (Blackwell Publishing Ltd, 2007).
43. Hall-Spencer, J., Rogers, A., Davies, J. & Foggo, A. Deep-sea coral distribution on seamounts, oceanic islands, and continental slopes in the Northeast Atlantic. *Bull. Mar. Sci.* **81,** 135–146 (2007).
44. Freiwald, A. *et al.* Global distribution of cold-water corals (version 3.0). Second update to the dataset in Freiwald et al. (2004) by UNEP-WCMC, in collaboration with Andre Freiwald and John Guinotte. Cambridge (UK): UNEP World Conservation Monitoring Centre. URL: http://data.unep-wcmc.org/datasets/3. (2017).
45. Velo, A. *et al.* A multiparametric method of interpolation using WOA05 applied to anthropogenic CO2 in the Atlantic. *Sci. Mar.* **74,** 21–32 (2010).
46. Locarnini, R. A. *et al.* World Ocean Atlas 2013, Volume 1: Temperature. *NOAA Atlas NESDIS* **73,** 40 (2013).
47. Zweng, M. . *et al.* World Ocean Atlas 2013, Volume 2: Salinity. *NOAA Atlas NESDIS* **74,** 39 (2013).
48. Garcia, H. E. *et al.* World Ocean Atlas 2013, Volume 3: Dissolved Oxygen, Apparent Oxygen Utilization, and Oxygen Saturation. *NOAA Atlas NESDIS* **75,** 27 (2014).
49. Garcia, H. E. *et al.* World Ocean Atlas 2013, Volume 4: Dissolved Inorganic Nutrients (phosphate, nitrate, silicate). *NOAA Atlas NESDIS* **76,** 25 (2014).
50. Khatiwala, S., Primeau, F. & Hall, T. Reconstruction of the history of anthropogenic CO_2 concentrations in the ocean. *Nature* **462,** 346–349 (2009).
51. Lherminier, P. *et al.* The Atlantic Meridional Overturning Circulation and the subpolar gyre observed at the A25-OVIDE section in June 2002 and 2004. *Deep Sea Res. Part Oceanogr. Res. Pap.* **57,** 1374–1391 (2010).
52. Gourcuff, C., Lherminier, P., Mercier, H. & Le Traon, P. Y. Altimetry Combined with Hydrography for Ocean Transport Estimation. *J. Atmospheric Ocean. Technol.* **28,** 1324–1337 (2011).

53. Daniault, N., Lherminier, P. & Mercier, H. Circulation and Transport at the Southeast Tip of Greenland. *J. Phys. Oceanogr.* **41,** 437–457 (2011).
54. Kriegler, E. *et al.* Fossil-fueled development (SSP5): An energy and resource intensive scenario for the 21st century. *Global Environmental Change* (2017). doi:http://dx.doi.org/10.1016/j.gloenvcha.2016.05.015

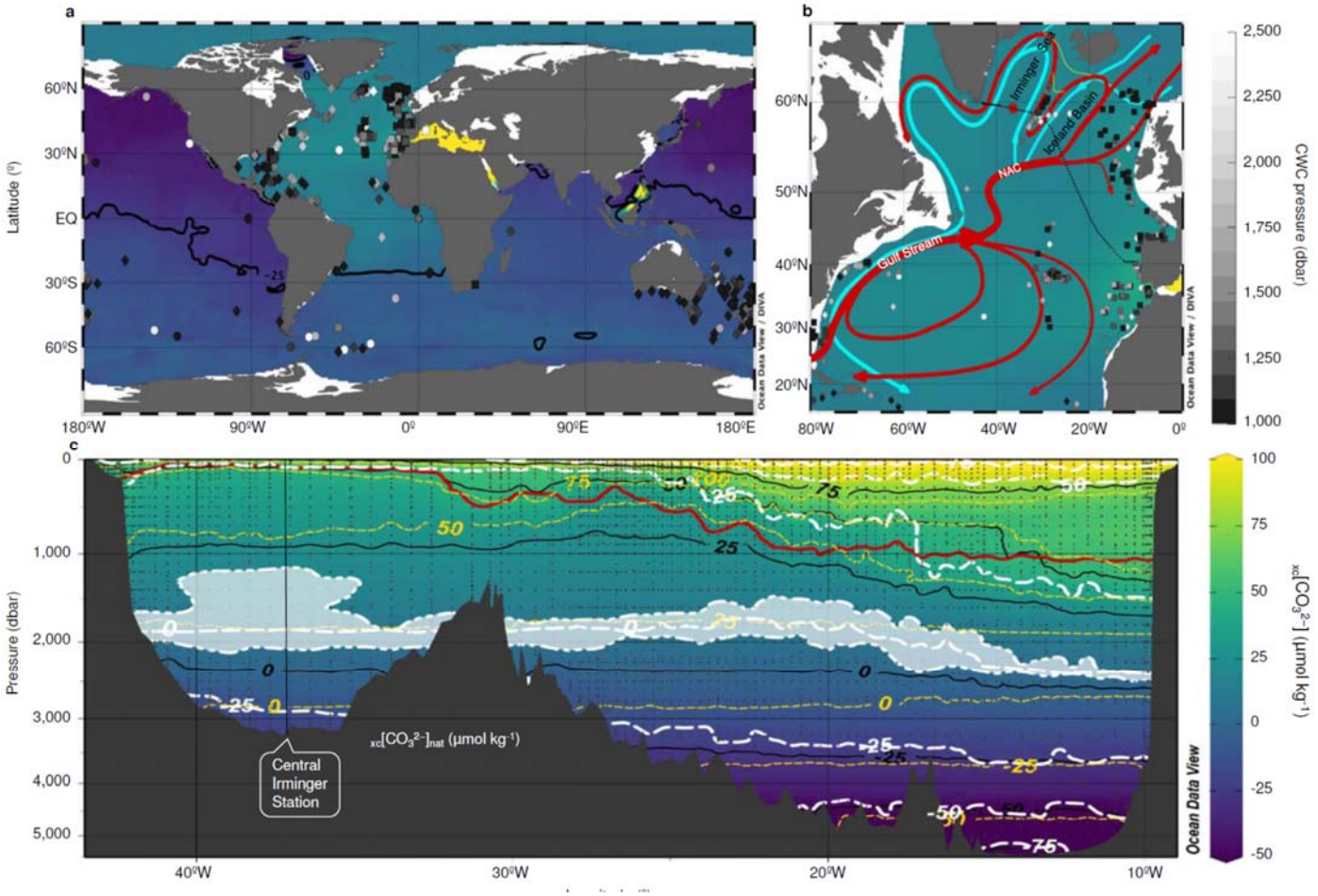

Figure 1 | Aragonite saturation and cold-water coral distribution. (a) $_{xc}[CO_3^{2-}]$ at 1,500 m (lower-right colorbar). Circles, diamonds and squares represent CWC locations where $_{xc}[CO_3^{2-}]<0$, $0<{}_{xc}[CO_3^{2-}]<25$, and $_{xc}[CO_3^{2-}]>25$ µmol kg^{-1}, respectively. Depths are gray-coded (upper-right colorbar). (b) Central Irminger Station (red star), Ovide section (dotted line) and circulation of upper (red) and lower (blue) AMOC limbs. (c) $_{xc}[CO_3^{2-}]$ observed (colour and black lines), natural (yellow-dashed lines), and for a doubling of present atmospheric C_{ant} (dashed-white line) along the Ovide section. The milky area is uncertainty for aragonite saturation horizon ($_{xc}[CO_3^{2-}]=0$). The red line separates the upper and lower AMOC limbs. Dots represent samples.

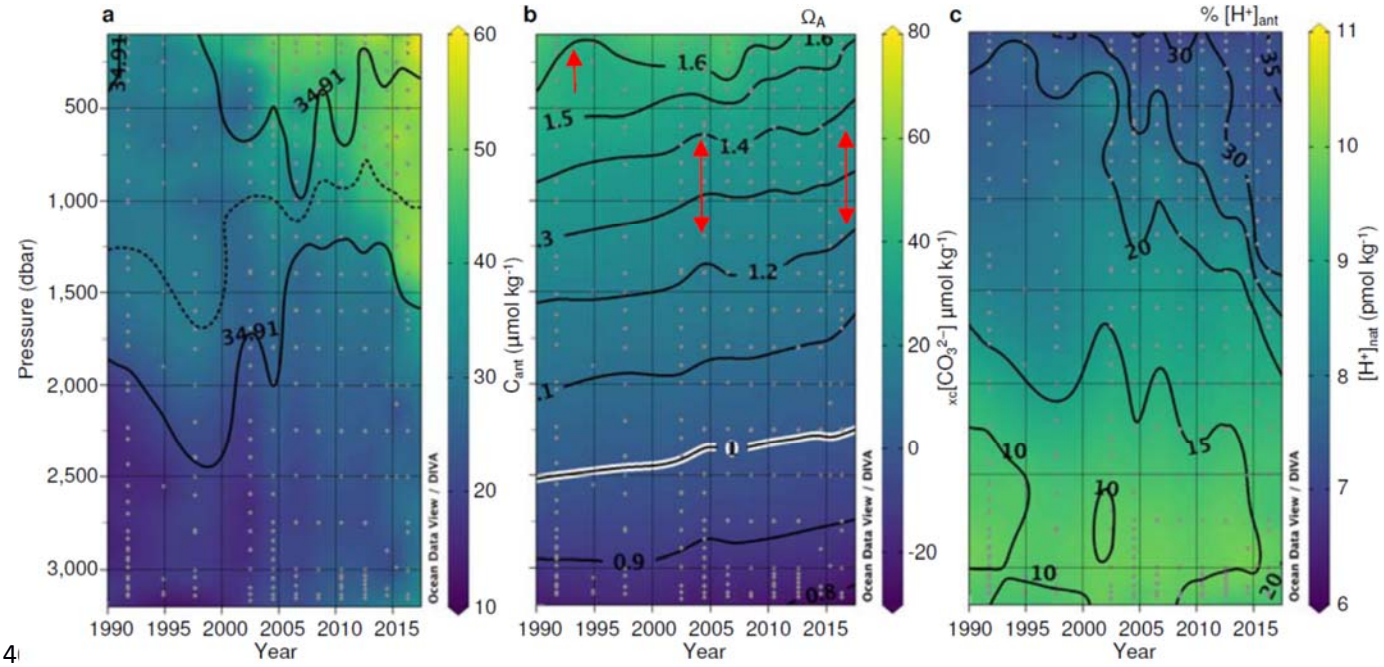

403 **Figure 2 | Ocean Acidification at the Central Irminger Station.** (a) Time evolution from
404 1991 to 2016 of anthropogenic CO_2 (C_{ant}, colorbar), the isohaline of 34.91 (continuous
405 black lines) and salinity minimum (dotted black line). (b) Time evolution from 1991 to
406 2016 of aragonite saturation (Ω_A, contours) and excess of carbonate ion concentration over
407 aragonite saturation ($_{xc}[CO_3^{2-}]$, colorbar). Arrows indicate the effects of deep convection
408 events. (c) Time evolution from 1991 to 2016 of natural (pre-industrial) hydrogenion
409 concentration ($[H^+]_{nat}$, colorbar, in pmol kg^{-1}) and percentage of change in $[H^+]$ due to
410 anthropogenic emissions (% $[H^+]_{ant}$, contours).

411

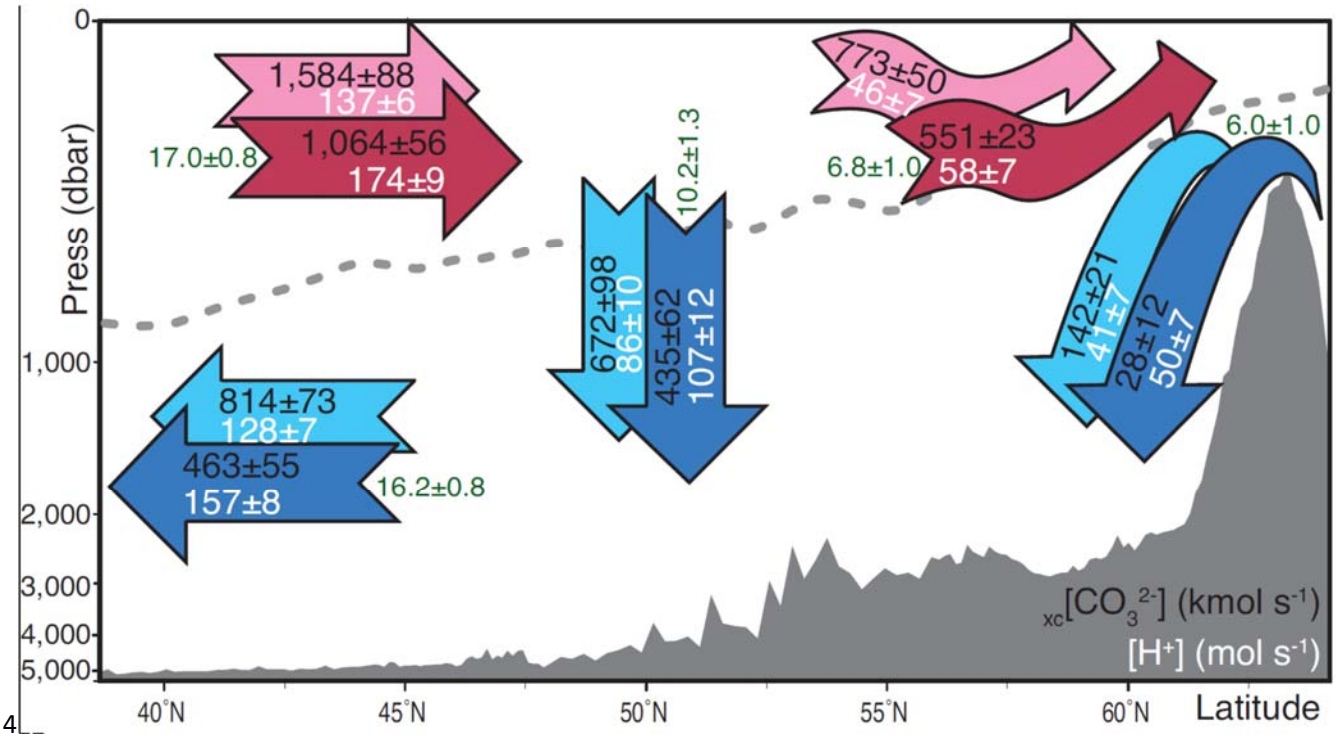

Figure 3 | Circulation of the excess of $[CO_3^{2-}]$ over aragonite saturation and $[H^+]$ in the Subpolar North Atlantic. Mean transports for 2002–2016 between the Ovide section and the Nordic Sills of seawater (green values, in Sv), and natural (pre-industrial; light coloured arrows) and observed (dark coloured arrows) excess of $[CO_3^{2-}]$ over aragonite saturation ($_{xc}[CO_3^{2-}]$, in kmol s^{-1}, black values) and hydrogenions ($[H^+]$, in mol s^{-1}, white values). Uncertainties are the errors in the mean transports across the eight occupations of the Ovide line (std/$\sqrt{8}$). The grey dotted line represents the limit between the upper and lower limbs of the AMOC.

Extended Data Legends

Extended Data Table 1 | Aragonite saturation at cold-water coral locations. Number (N) of locations of cold-water corals (CWC) in the Global and North Atlantic (NA) Oceans below 1,000 and 1,500 m, along with the percentage of the CWC located below the aragonite saturation horizon (ASH) for natural (pre-industrial; subscript 'nat'), present (subscript '2010') and for the doubling of atmospheric C_{ant} scenario (subscript '2x'). The average natural, measured (GLODAPv2)[12,13] and for the doubling of atmospheric C_{ant} scenario excess of carbonate ion concentration over aragonite saturation ($_{xc}[CO_3^{2-}]$, in µmol kg^{-1}) are also shown.

Depth (m)	Ocean	N	$<ASH_{nat}$	$<ASH_{210}$	$<ASH_{2x}$	$xc[CO3^{2-}]_{nat}$	$xc[CO3^{2-}]_{2010}$	$xc[CO3^{2-}]_{2x}$
≥1000	Global	548	12%	17%	47%	29	14.5	4
	NA	335(61%)	1%	2%	32%	43	24.5	10.5
≥1500	Global	176	20%	22%	74%	22	6.7	-8
	NA	139(78%)	2%	4%	70%	34	15	-3

Extended Data Table 2 | Transports of seawater, $_{xc}[CO_3^{2-}]$, $[H^+]$, C_{ant} and $[CO_3^{2-}]$. Transport of volume (in Sv; 1 Sv = 10^6 m^3 s^{-1}), anthropogenic CO_2 (C_{ant}, in kmol s^{-1}), carbonate ion concentration ($[CO_3^{2-}]$, in kmol s^{-1}), excess of carbonate ion concentration over aragonite saturation ($_{xc}[CO_3^{2-}]$, in kmol s^{-1}), and hydrogen ion concentration ($[H^+]$, in pmol s^{-1}) across the Ovide section during 2002–2016 in the upper and lower limbs of the Atlantic Meridional Overturning Circulation (AMOC). Values of the natural (pre-industrial) component (subscript 'nat') and for the doubling of atmospheric C_{ant} scenario (subscript '2x') are also shown. Uncertainties (*Err_x*) are estimated as the error of the mean of the eight occupations of the Ovide section (std/$\sqrt{8}$). Positive (negative) transports indicate northward (southward) transport. The velocity-weighted averaged values of $_{xc}[CO_3^{2-}]$ for pre-industrial, present (2002–2016) and for the doubling of atmospheric C_{ant} scenario are also given.

Year	Vol (Sv)	C_{ant} (kmol·s^{-1})	$[CO_3^{2-}]$ (kmol·s^{-1})	$[CO_3^{2-}]_{nat}$ (kmol·s^{-1})	$_{xc}[CO_3^{2-}]$ (kmol·s^{-1})	$_{xc}[CO_3^{2-}]_{nat}$ (kmol·s^{-1})	$_{xc}[CO_3^{2-}]_{2x}$ (kmol·s^{-1})	$[H^+]$ (pmol·s^{-1})	$[H^+]_{nat}$ (pmol·s^{-1})	$[H^+]_{2x}$ (pmol·s^{-1})
AMOC upper limb										
2002	17.3	761	2,322	2,784	1,058	1,520	737	177	144	209
2004	17.15	820	2,409	2,910	1,172	1,673	823	172	138	205
2006	11.97	528	1,596	1,917	743	1,064	520	119	97	141
2008	17.14	886	2,412	2,954	1,173	1,716	795	171	135	206
2010	18.03	919	2,477	3,037	1,166	1,727	776	187	148	225
2012	16.51	819	2,116	2,609	922	1,415	578	172	135	208
2014	18.75	1,048	2,563	3,200	1,199	1,837	755	189	147	230
2016	19.04	1,068	2,468	3,114	1,078	1,724	628	201	154	247
Avg.	**17**	**856**	**2,295**	**2,816**	**1,064**	**1,584**	**701**	**174**	**137**	**209**
Err_x	**0.78**	**61**	**110.3**	**144.2**	**56**	**88**	**39**	**9**	**6**	**11**
Velocity-weighted averaged $_{xc}[CO_3^{2-}]$					**61±2**	**90±2**	**40±1.4**			
AMOC lower limb										
2002	-16.5	-548	-1,920	-2,240	-640	-960	-417	-151	-127	-175
2004	-16.3	-547	-1,812	-2,128	-454	-770	-233	-156	-130	-181
2006	-11.2	-343	-1,294	-1,495	-357	-557	-218	-106	-90	-121
2008	-16.3	-694	-1,899	-2,305	-680	-1,087	-397	-150	-120	-180
2010	-17.2	-567	-1,913	-2,239	-288	-614	-60	-175	-147	-202
2012	-15.7	-646	-1,769	-2,144	-524	-899	-263	-151	-121	-181
2014	-17.9	-636	-1,899	-2,262	-259	-622	-6	-184	-151	-215
2016	-18.2	-882	-1,957	-2,465	-500	-1,007	-146	-184	-140	-226
Avg.	**-16.2**	**-608**	**-1,808**	**-2,160**	**-463**	**-814**	**-217**	**-157**	**-128**	**-185**
Err_x	**0.78**	**43**	**84.8**	**106**	**55**	**73**	**46**	**8**	**7**	**10**
Velocity-weighted averaged $_{xc}[CO_3^{2-}]$					**28±3**	**49±4**	**13.6±2.7**			

Extended Data Table 3 | Transports at the Nordic Sills. Volume transport (Vol., in Sv), potential temperature (Tpot, in ºC), salinity, total dissolved inorganic carbon (C_T, in µmol kg^{-1}), total alkalinity (A_T, in µmol kg^{-1}), anthropogenic CO_2 (C_{ant}, in µmol kg^{-1}), carbonate ion concentration ([CO_3^{2-}], in µmol kg^{-1}), excess of carbonate ion concentration over aragonite saturation ($_{xc}$[CO_3^{2-}], in µmol kg^{-1}), and hydrogen ion concentration ([H^+], in pmol kg^{-1}) through the Nordic Sills in the upper and lower limbs of the AMOC, separated by isopycnal 1,027.8 kg m^{-3}. Values for the natural (pre-industrial) component (subscript 'nat') are also shown. Salinity and marine CO_2 system data (C_T and A_T) taken from Jeansson et al.[17]. Volume transports taken from Pérez et al.[19]. AW, OW and PW stand for Atlantic, Overflow and Polar Waters, respectively; and the subscripts stand for: Faroes-Shetland, between Faroes and Shetland islands; Iceland-Faroe, across the Iceland-Faroe Ridge; W-Iceland, West of Iceland; and Denmark Strait, through Denmark Strait. Uncertainties of volume transport, salinity, C_T, C_{ant} and A_T taken from Jeansson et al. [18]. The uncertainties of C_T and A_T were propagated to [CO_3^{2-}] and [H^+] by a Monte-Carlo approach using the marine CO_2 system equations.

Layer	Vol (Sv)	Tpot (ºC)	Salinity	C_T (µmol·kg^{-1})	A_T (µmol·kg^{-1})	C_{ant} (µmol·kg^{-1})	[CO_3^{2-}] (µmol·kg^{-1})	[CO_3^{2-}]$_{nat}$ (µmol·kg^{-1})	$_{xc}$[CO_3^{2-}] (µmol·kg^{-1})	$_{xc}$[CO_3^{2-}]$_{nat}$ (µmol·kg^{-1})	[H^+] (pmol·kg^{-1})	[H^+]$_{nat}$ (pmol·kg^{-1})
AMOC upper limb (Density <27.8)												
$AW_{Faroes-Shetland}$	3.9±0.5	9.18±0.55	35.27±0.11	2,121±20	2,325±7	50±3	146±8	176±10	76±8	107±10	8.0±0.9	6.4±1.0
$AW_{Iceland-Faroe}$	3.9±0.5	8.10±0.30	35.18±0.06	2,127±22	2,323±6	47±3	140±10	169±12	70±10	99±12	8.0±1.1	6.4±1.3
$AW_{W-Iceland}$	0.8±0.16	6.00±0.15	35.06±0.03	2,138±3	2,309±2	48±2	124±2	153±2	54±2	83±2	8.4±0.1	6.6±0.2
$PW_{Denmark\ Strait}$	-1.8±0.5	-0.91±1.35	34.07±0.27	2,114±8	2,266±3	38±1	110±3	132±4	42±3	64±4	6.9±0.4	5.6±0.5
AMOC upper limb (Density >27.8)												
$OW_{Faroes-Shetland}$	-2.0±0.3	0.59±0.10	34.91±0.02	2,163±3	2,303±3	27±6	100±2	115±4	2±2	17±4	8.1±0.0	7.0±0.5
$OW_{Iceland-Faroe}$	-1.0±0.5	0.33±0.30	34.89±0.06	2,156±5	2,304±8	33±4	104±2	123±5	6±2	25±5	7.7±0.2	6.4±0.1
$OW_{Denmark\ Strait}$	-3.0±0.3	1.47±0.45	34.86±0.09	2,148±6	2,294±5	37±2	104±2	124±3	6±2	27±3	8.1±0.1	6.6±0.2

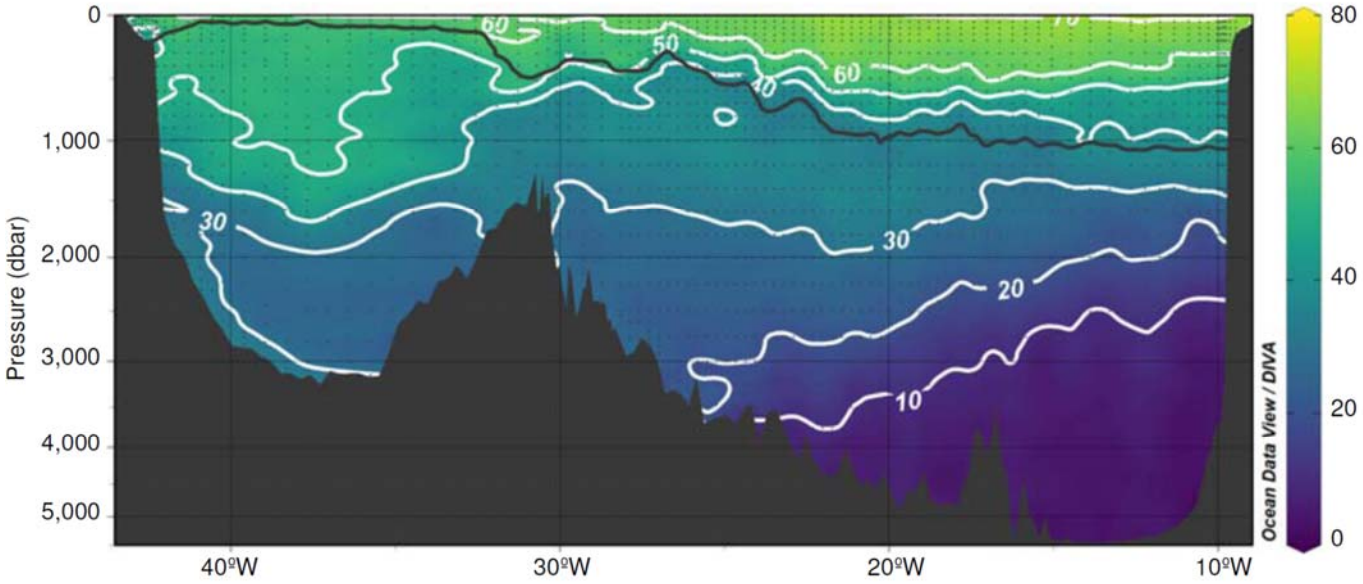

466 **Extended Data Figure 1 | Anthropogenic CO_2 along the 2016 Ovide section.** Vertical
467 distribution of anthropogenic CO_2 (in µmol kg^{-1}) along the Ovide section (Fig. 1b) in 2016.
468 The black line is the isopycnal delimiting the upper and lower limbs of the AMOC.

469

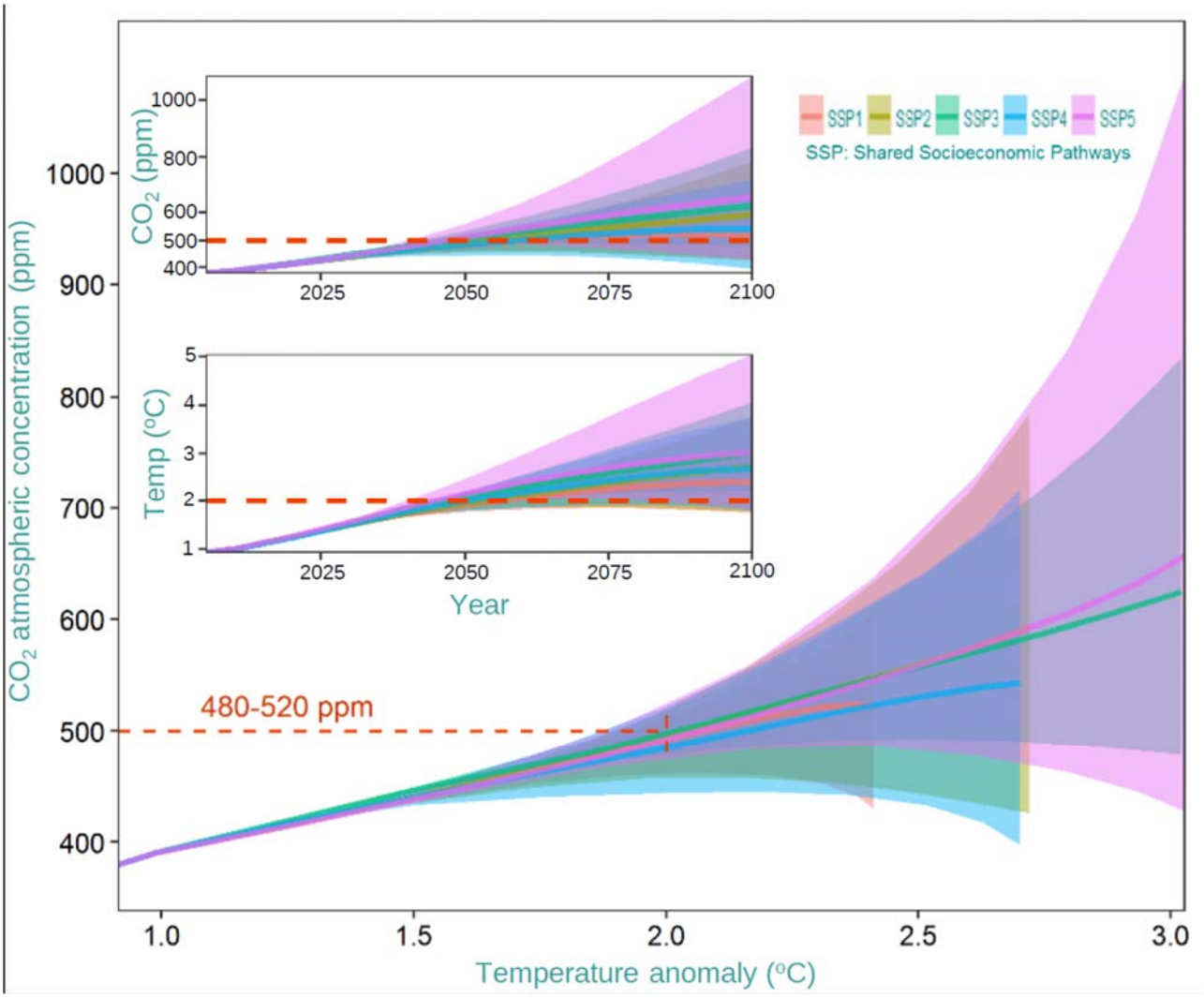

471 **Extended Data Figure 2 | Projections of atmospheric CO_2 and temperature change of**
472 **the five Shared Socioeconomic Pathways (SPP)[24].** Present: 1°C warming with
473 atmospheric CO_2 concentration ($[CO_2^{atm}]$) of 400 ppm[21], which represents an atmospheric
474 CO_2 excess ($_{xc}[CO_2^{atm}]$) of 120 ppm ($_{xc}[CO_2^{atm}] = [CO_2^{atm}] - 280$ ppm; where 280 ppm is
475 the pre-industrial $[CO_2^{atm}]$). The doubling of atmospheric C_{ant} scenario, i.e. 2 x present-day
476 $_{xc}[CO_2^{atm}]$ (480–520 ppm), is within the projection range for a 2°C-warming scenario,
477 which could be reached in 2040–2052 according to SSP5 (pink shadowed area). SSP5 is the
478 only scenario that results in a radiative forcing as high as the former RCP8.5
479 (Representative Concentration Pathways)[54].

480

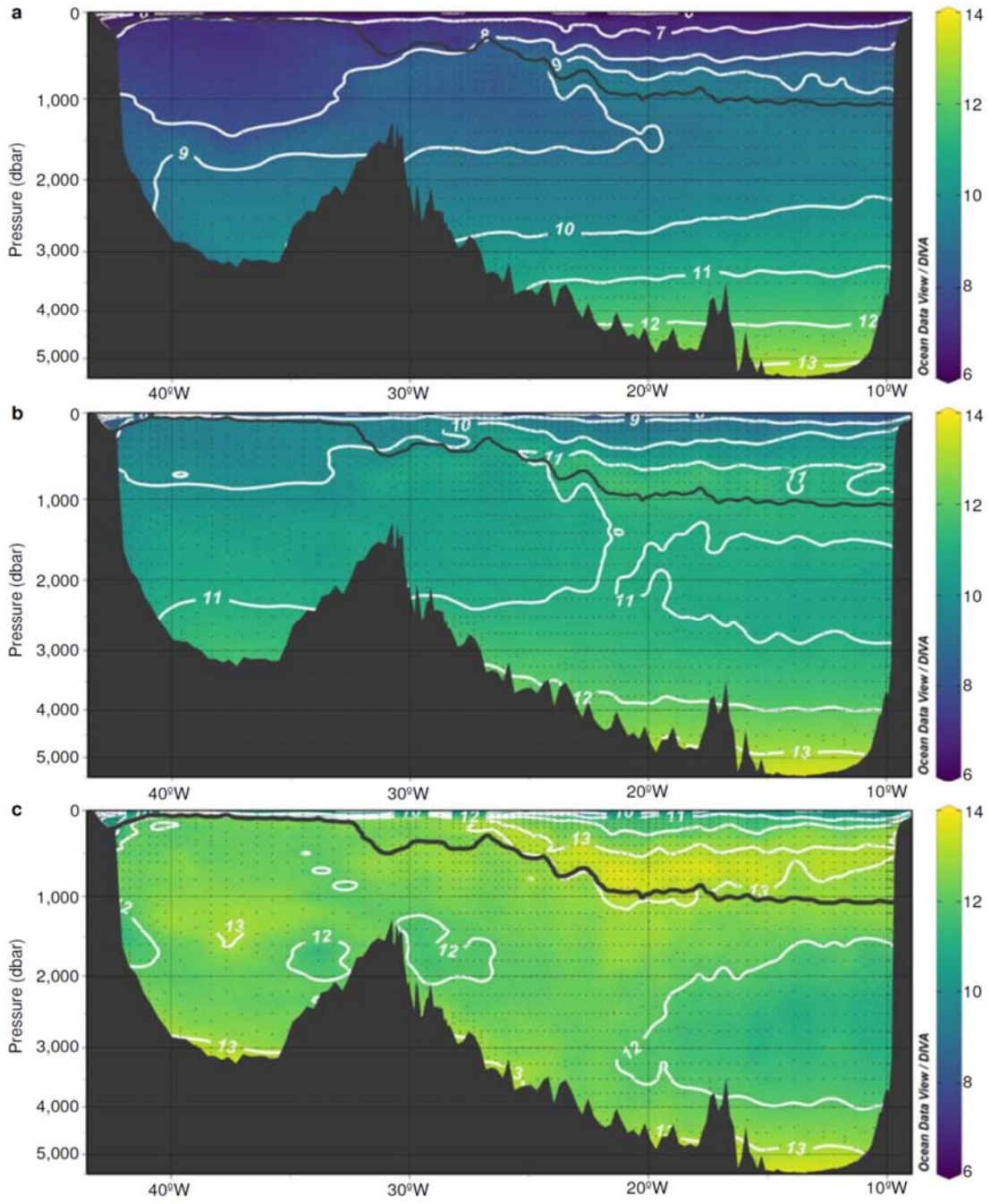

Extended Data Figure 3 | Evolution of ocean acidification from pre-industrial to the doubling of atmospheric C_{ant} scenario. Hydrogen ion concentrations ($[H^+]$, in pmol kg^{-1}) along the Ovide section (Fig. 1b) for the (a) pre-industrial, (b) present (2016) and (c) doubling of atmospheric C_{ant} scenario. The black line is the isopycnal delimiting the upper and lower limbs of the AMOC.

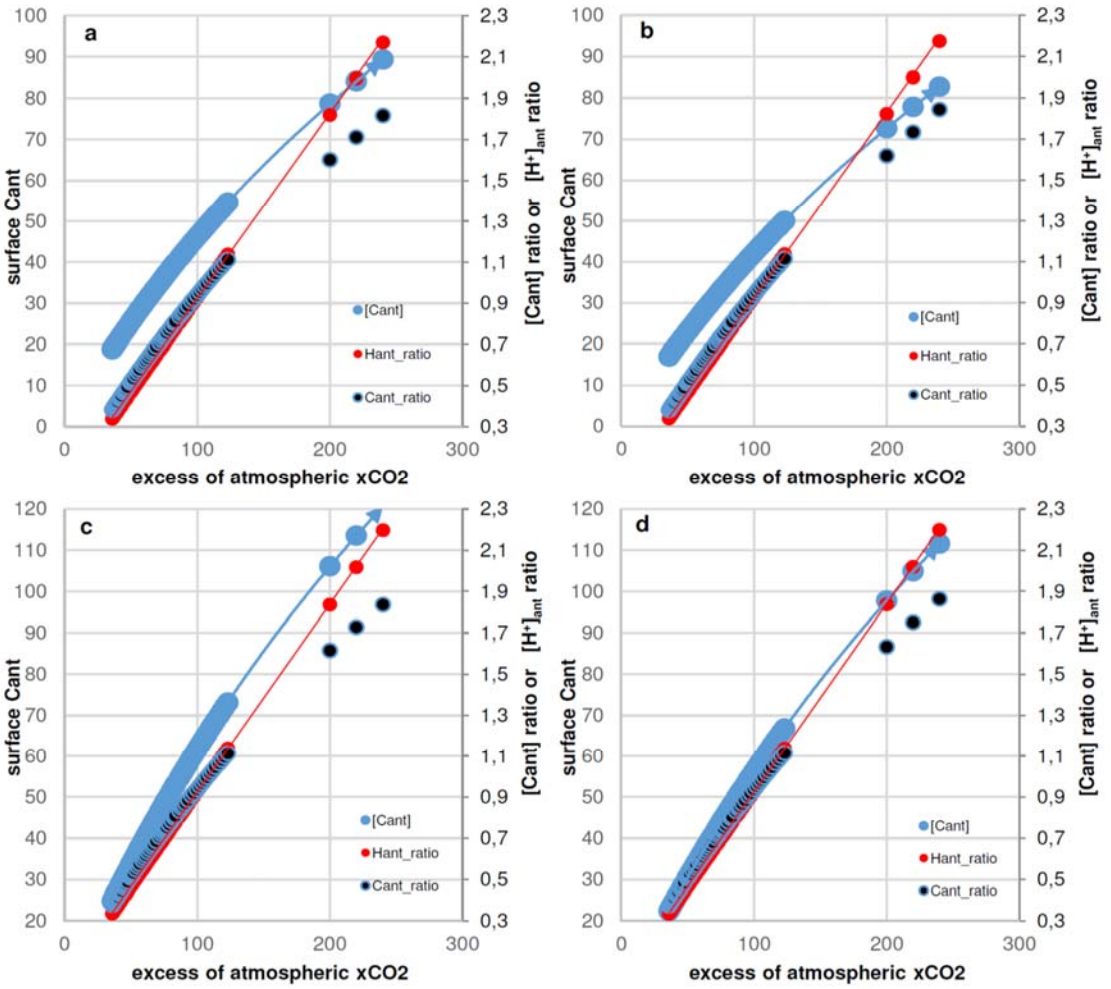

Extended Data Figure 4 | Progression of anthropogenic CO_2 in surface waters versus excess of atmospheric xCO_2 at different temperatures and CO_2 disequilibriums. Concentration of anthropogenic CO_2 ($[C_{ant}]$, light blue dots, in µmol kg^{-1}), Cant_ratio (navy dots) and Hant_ratio (red dots) versus the excess of atmospheric xCO_2 due to anthropogenic signal during 1959–2016 for (a) 2ºC and 5% of CO_2 disiquilibrium, (b) 2ºC and 15% of CO_2 disiquilibrium, (c) 20ºC and 5% of CO_2 disiquilibrium, and (d) 20ºC and 15% of CO_2 disiquilibrium. The Cant_ratio (Hant_ratio) is the ratio between the $[C_{ant}]$ ($[H^+]_{ant}$) at any time and the average $[C_{ant}]$ ($[H^+]_{ant}$) for the Ovide period (2002–2016). The computed values for the doubling of atmospheric C_{ant} scenario (excess of atmospheric xCO_2 of 220 ± 20 ppm) are also shown. The progression of the Hant_ratio fits to a straigh line, while, the Cant_ratio decreases when increasing the atmospheric xCO_2 due to the buffer capacity of the marine CO_2 system (Revelle factor). An increase of 72 ± 3% in C_{ant} above the average $[C_{ant}]$ for the Ovide period (2002–2016) is computed for the doubling of atmospheric C_{ant} scenario. This is practicaly independent of the seawater temperature and the degree of CO_2 disiquilibrium[41].

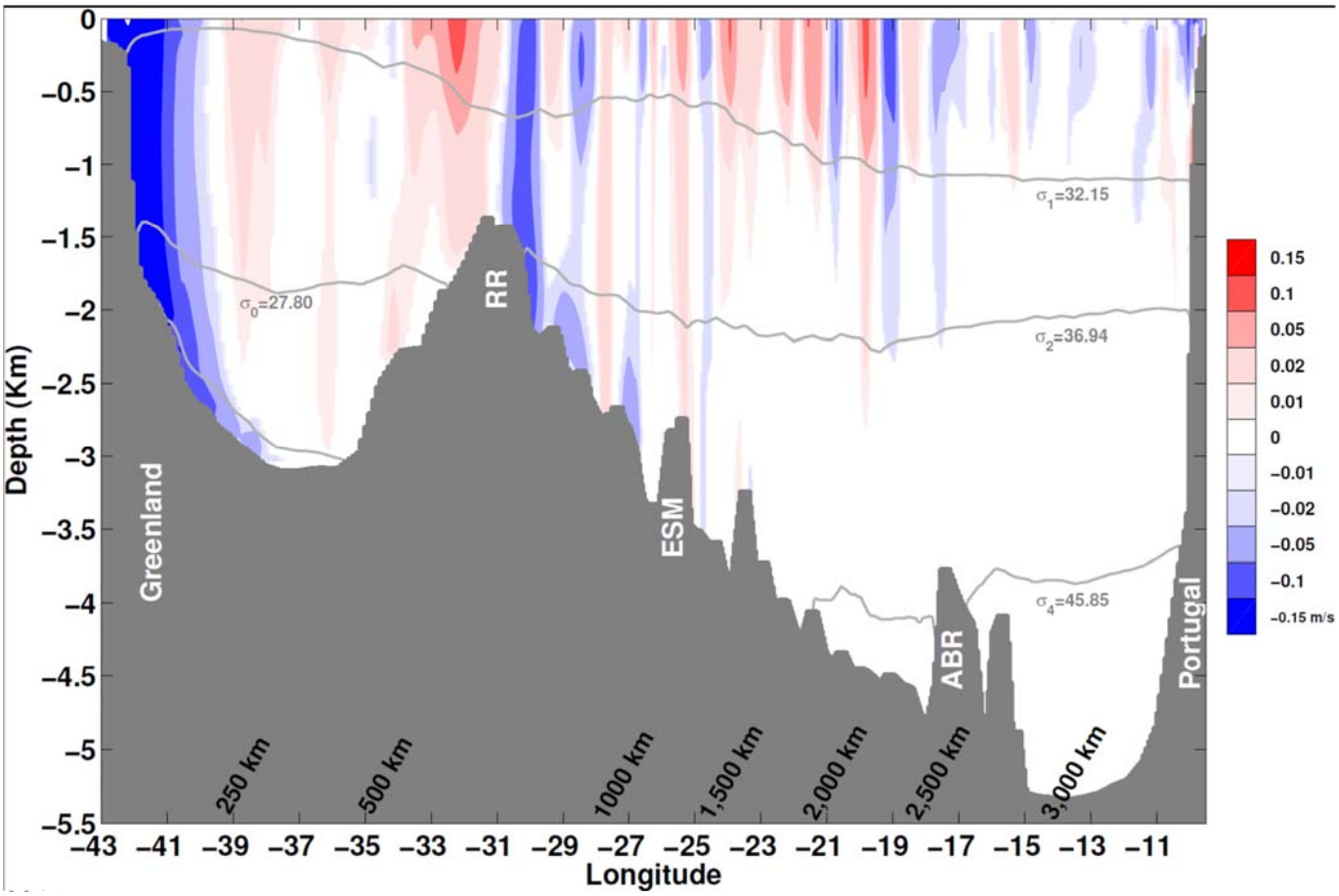

Extended Data Figure 5 | Mean velocities orthogonal to Ovide. Mean velocities (in m s^{-1}) orthogonal to the Ovide section for the period 2002–2016. The Ekman velocities, estimated from winds stress averaged over the months of the cruises and equally distributed over the first 30 m, were added to the geostrophic velocities derived from a box inverse model[17,51–53]. Positive (negative) velocities indicate northeastward (southwestward) currents. The horizontal grey lines are the isopycnals σ_1 = 32.15 kg m^{-3}, σ_2 = 36.94 kg m^{-3} and σ_4 = 45.85 kg m^{-3}. The km at the bottom of the figure indicates distance from Greenland. The acronyms indicate topographic features: Reykjanes Ridge (RR), Eriador Seamount (ESM) and Azores-Biscay Ridge (ABR).

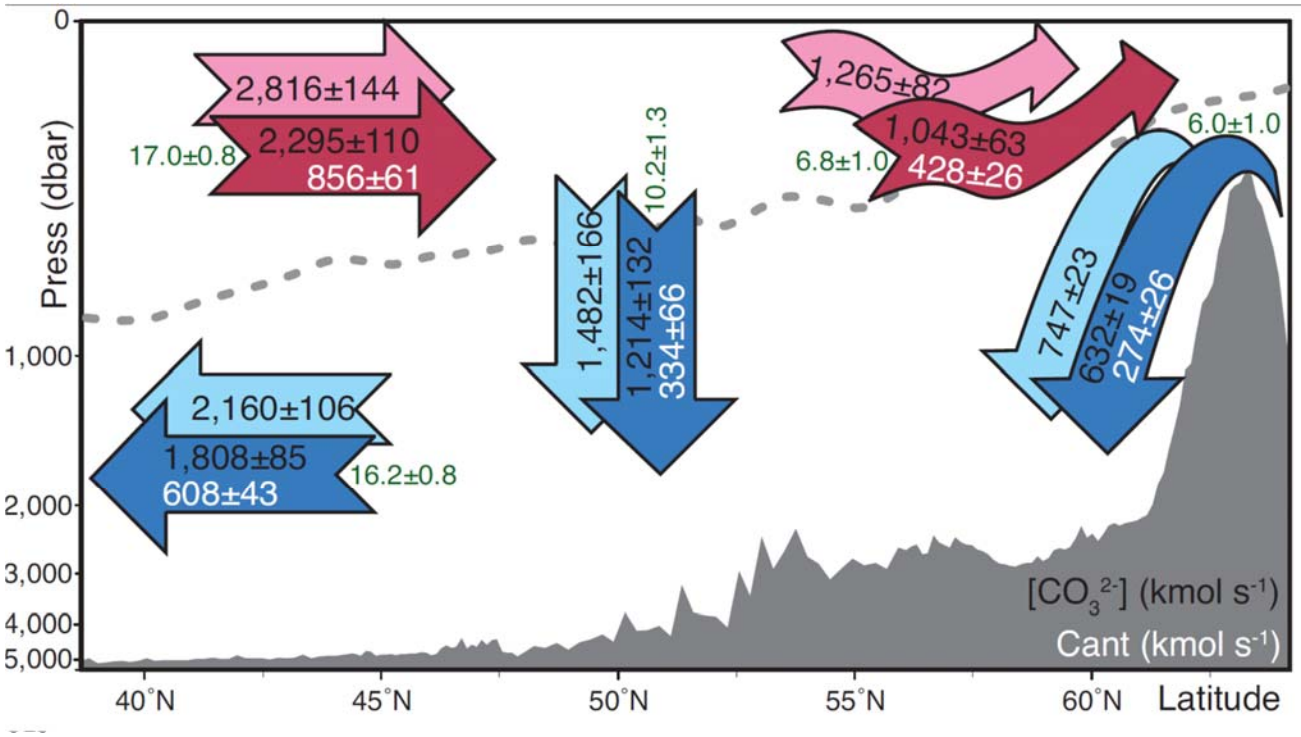

Extended Data Figure 6 | Circulation of carbonate ions and anthropogenic CO_2 in the Subpolar North Atlantic. Mean transports for 2002–2016 between the Ovide section and the Nordic Sills of seawater (green values, in Sv), and natural (pre-industrial; light coloured arrows) and observed (dark coloured arrows) carbonate ion concentration ($[CO_3^{2-}]$, in kmol s^{-1}, black values) and anthropogenic CO_2 (C_{ant}, in kmol s^{-1}, white values). Uncertainties are the errors of the mean transports across the eight occupations of the Ovide section (std/$\sqrt{8}$). Transports at the Nordic Sills derived from Jeansson et al.[18] and Pérez et al.[19]. The grey dotted line represents the limit between the upper and lower limbs of the AMOC.

Data availability: OVIDE cruise data from 2002 to 2010 are part of GLODAPv2 data product available at CDIAC Ocean CO_2 Data (http://cdiac.ornl.gov/oceans). OVIDE 2012 data was accessed from the Clivar & Carbon Hydrographic Data Office (CCHDO; http://cchdo.ucsd.edu/cruise/29AH20120622), and OVIDE 2014 data is publicly available at http://www.obs-vlfr.fr/proof/ftpfree/geovide/ALKALINITY_PH/. The OVIDE

2016 data that support the findings of this study are available at http://dx.doi.org/10.20350/digitalCSIC/8513.

Acknowledgments

The OVIDE research project was co-funded by IFREMER and CNRS/INSU/LEFE. H.M. was supported by CNRS. This is a contribution to AtlantOS project funded by the European Union's Horizon 2020 research and innovation programme under grant agreement No 633211. This study is also a contribution to the project BOCATS (CTM2013-41048-P) supported by the Spanish Ministry of Economy and Competitiveness and co-funded by the Fondo Europeo de Desarrollo Regional 2014–2020 (FEDER). We are grateful to the Captain of Sarmiento Gamboa, Anxeles Campos, and her crew for invaluable help that make possible the success of the BOCATS cruise. We are grateful to Des Barton for the English revision.

Author contributions

F.F.P., M.F., M.I.G-I. and H.M. contributed equally to this paper. F.F.P., H.M. and P.L. designed the program and F.F.P., H.M. and P.L. executed the field work. F.F.P, M.F., M.I.G-I., A.V., M.P., F.A-P., E.F.G. and X.A.P. contributed to the chemical determination of nutrients and carbon system. H.M., P.L. and P.Z. contributed with the currents measurements and inverse model results. All authors contributed to discussion and writing.

Competing financial interests

The authors declare no competing financial interests.

Additional information

Supplementary information is available in the online version of the paper. Reprints and permissions information is available online at www.nature.com/reprints. Correspondence and requests for materials should be addressed to F.F.P. (fiz.perez@iim.csic.es)